Mathematics

AIMS Mathematics, 10(7): 15955–15974.
DOI: 10.3934/math.2025715
Received: 09 May 2025
Revised: 23 June 2025
Accepted: 23 June 2025
Published: 16 July 2025

http://www.aimspress.com/journal/Math

Research article

Mathematical analysis for bioconvection peristaltic transport of Sutterby nanofluid with chemical reaction

Zahid Nisar[1,*] and Humaira Yasmin[2,3,*]

[1] Department of Computer Science, National University of Sciences and Technology (NUST), Balochistan Campus (NBC), Quetta 87300, Pakistan
[2] Department of Basic Sciences, General Administration of Preparatory Year, King Faisal University, P.O. Box 400, Al Ahsa, 31982, Saudi Arabia
[3] Department of Mathematics and Statistics, Faculty of Science, King Faisal University, P.O. Box 400, Al Ahsa, 31982, Saudi Arabia

* **Correspondence:** Email: zahidnisar@nbc.nust.edu.pk; hhassain@kfu.edu.sa.

Abstract: The current investigation deals with the bioconvective peristaltic flow of a Sutterby nanofluid in a channel. Here, symmetric channel walls are considered to be elastic. Thermal transport included effects such as thermal radiation, Joule heating, and dissipation. The characteristics of a first-order chemical reaction are integrated into mass transport. We utilized a large wavelength approximation with a small Reynolds number to simplify the system. After that, we used numerical techniques for the solution of a complex system of equations. Finally, the effects of several parameters are examined graphically. This research could have a big influence on optimizing heat and mass transfer in nanofluid-based systems, with potential implications for solar energy systems, thermal management devices, biosensors, fuel cell technology, pharmaceutical processing, and targeted drug delivery mechanisms.

Keywords: peristalsis; bioconvection; nanomaterial; sutterby fluid; chemical reaction
Mathematics Subject Classification: 76A02, 76A05, 65L10, 80A21, 80A32

1. Introduction

Nanofluids are liquids infused with tiny particles (less than 100 nanometers) that have recently become a hot research topic. Because of their special qualities, nanofluids are used in many industrial and medical applications. Because of their low viscosity and superior thermal conductivity, which reduces friction and dissipates heat during operations, they are useful lubricants and cooling agents in surgical procedures. In addition to the medical field, nanofluids are used in nuclear reactors, solar energy systems, fuel cell technology, drug delivery systems, geothermal technology, biomedical imaging, and increased oil recovery. Choi et al. [1] provided experimental data demonstrating improved thermal performance when compared to the base liquid, as a result of the dispersion of nanoparticles. After that, Buongiorno [2] extended this concept; in this study, he incorporated the features of Brownian motion and thermophoresis. The presence of these effects significantly increases both the viscosity and thermal conductivity of the base fluid, resulting in a considerable improvement in heat transfer efficiency. Godson et al. [3] explored how nanofluids are useful tools for heat transfer enhancement. Hussein et al. [4] investigated nanofluids in automotive cooling systems. Hayat and Nadeem [5] analyzed the enhancement in the heat transfer by a hybrid nanofluid. The peristaltic movement of Jeffrey six-constant nanofluid was studied by Imran et al. [6]. Abbasi and Shehzad [7] described the magnetohydrodynamic (MHD) peristaltic flow in a curved nature channel containing nanomaterials. Ajithkumar et al. [8] examined the peristaltic flow of Bingham nanofluid through a porous space. Nisar et al. [9] studied the implications of thermal radiation on the peristaltic motion of a couple stress magnetic nanofluid. Ajithkumar et al. [10] discussed the peristalsis of a Sutterby nanofluid with a chemical reaction. Further research on this subject is available in [11–13].

Peristalsis is characterized as a wave-like, progressive motion that happens as a wave moves through a duct or tube or along a channel's edge. This process involves fluid movement resulting from wave propagation, specifically caused by the passage of curving waves along a path. Researchers are particularly interested in peristalsis due to its significant applications in areas such as nuclear reactors, physiology, combustion, turbomachinery, and fluid pumping driven by sinusoidal wave propagation. It also plays an important role in moving genetic material, such as sperm and ova, to their corresponding tubes in the male and female reproductive organs. Engineers use peristaltic systems for a variety of purposes, the most popular being pumping, as a result of biomimicry and bioinspired engineering. Multiple waves of peristalsis force fluid through a tube, which makes this process efficient. Latham [14] was the first to investigate the peristaltic movement through both experimental and theoretical approaches. Shapiro et al. [15] expanded on this concept by examining the case of low Reynolds numbers and applying a long-wavelength approximation. The role of peristalsis in pharmacological and physiological characteristics in the small intestines was studied by Trendelenburg [16]. Bandopadhyay et al. [17] examined peristaltic flow in microfluidic channels. Chemically reactive Sutterby liquid peristaltic movement was analyzed by Imran et al. [18]. Akram et al. [19] investigated radiative MHD peristaltic movement for Prandtl nanofluid with double diffusion convection. Nisar et al. [20] discussed the aspects of entropy generation for the peristaltic flow of fourth-grade nanofluid. Alahmadi et al. [21] investigated the peristaltic flow of nanomaterials with an artificial neural network. Srinivas et al. [22] analyzed thermal features considering the peristalsis of particle-liquid suspension. Ishaq et al. [23] examined the peristaltic motion for Johnson-Segalman nanofluid via an artificial neural network.

Numerous engineering, commercial, and biological applications use a variety of non-Newtonian fluids for cooling procedures. Given how often these fluids are used, a detailed analysis of their rheological characteristics is required. Oils, coatings, polymer melts, fuel, and suspensions are examples of complicated fluids whose behavior is not well described by the standard Navier-Stokes equation. These fluids' rheological properties are well-represented by the power-law fluid model. Sutterby proposed an idea in 1966 [24] that described the viscosity data of several polymer melts and solutions and identified a non-Newtonian fluid designated as the Sutterby fluid. Comprehending Sutterby fluids is crucial for tackling real-world problems in a wide range of businesses, technical specialties, and physiological research. This multidisciplinary aspect of the field makes it preferred over conventional viscous fluid investigations. Akbar and Nadeem [25] explored the aspects of the peristaltic flow of a Sutterby fluid through the small intestines. Abdelsalam et al. [26] examined the activation energy features of peristaltic motion with a Sutterby fluid. Chinnasamy et al. [27] studied the artificial neural network model for the peristalsis of a Sutterby fluid with nanomaterials. Revathi et al. [28] examined the activity of a Sutterby fluid. Ali et al. [29] investigated the numerical inquiry for bioconvective Sutterby nanomaterials through a rotating disk.

Researchers are very interested in studying microorganism bioconvection because of its many potential uses. The term "bioconvection" [30] describes the grouping of microorganism-containing fluid inside the medium under study. Bacteria, algae, and fungi are a few types of these microorganisms. Microorganisms moving randomly in the form of cell colonies are what define the process. The existence of microorganisms that are denser than the neighboring fluid, such as water, causes them to climb, which is the primary source of this phenomenon. Microbial migration originates from unstable and irregular patterns in the higher layers. Bacteria provides an excellent model system for studying microorganism bioconvection because of this phenomenon, which has many uses in biochemistry and bioengineering. Some recent activity in this area can be seen via [31–33].

The primary objective of this study is to investigate the bioconvective radiative peristaltic behavior of a Sutterby nanofluid. The analysis employs the Buongiorno nanofluid model, incorporating the influences of thermophoresis and Brownian motion. Assumptions of long wavelength and low Reynolds number are considered. Slip boundary conditions are applied within an elastic, symmetric channel. The study also accounts for Joule heating, viscous dissipation, and a first-order chemical reaction. A simplified set of governing equations is solved using a numerical method, and the impact of key parameters is illustrated through graphical analysis.

2. Mathematical modeling of the problem

Here, we study the two-dimensional chemically reactive peristaltic transport of a Sutterby nanoliquid in the presence of motile microorganisms. The current study also incorporates magnetic effects. Thermal transfer is additionally influenced by viscous dissipation, Joule heating, and thermal radiation. Further, the sinusoidal wave of length λ propagates in the horizontal direction of the flexible channel. The symmetric channel walls (having length d_1) are defined below [9]

$$y = \pm\eta(x,t) = \pm[d_1 + a\sin\frac{2\pi}{\lambda}(x - ct)], \tag{1}$$

where c is the wave speed, and t and a the time and amplitude, respectively. The stress tensor for the Sutterby liquid is outlined by [24].

$$S = \frac{\mu}{2}\left[\frac{\sinh^{-1}(\dot{\gamma}b)}{\dot{\gamma}b}\right]^{m^*}\mathbf{A}_1, \tag{2}$$

$$\dot{\gamma} = \sqrt{\frac{1}{2}trace\mathbf{A}_1^2}, \tag{3}$$

here, μ is the dynamic fluid viscosity, and m^* and b constants of the material. Further, the first Rivlin-Ericksen tensor $\mathbf{A}_1$ is defined as

$$A_1 = (grad\, V) + (grad\, V)^t. \tag{4}$$

The governing equations of the related problem are [2,10,32]

$$\frac{\partial u}{\partial x} + \frac{\partial v}{\partial y} = 0, \tag{5}$$

$$\begin{aligned}\rho_f\left(\frac{\partial u}{\partial t} + u\frac{\partial u}{\partial x} + v\frac{\partial u}{\partial y}\right) &= -\frac{\partial p}{\partial x} + \frac{\partial S_{xx}}{\partial x} + \frac{\partial S_{xy}}{\partial y} - \sigma B_0^2 u \\ &+ g(1-F_0)\rho_f\beta_T(T-T_0) - (\rho_p-\rho_f)g\beta_c(C-C_0) - (\rho_m-\rho_f)\gamma g(F-F_0),\end{aligned} \tag{6}$$

$$\rho_f\left(\frac{\partial v}{\partial t} + u\frac{\partial v}{\partial x} + v\frac{\partial v}{\partial y}\right) = -\frac{\partial p}{\partial y} + \frac{\partial S_{yx}}{\partial x} + \frac{\partial S_{yy}}{\partial y} - \sigma B_0^2 v, \tag{7}$$

$$\begin{aligned}\rho_f c_f\left(\frac{\partial T}{\partial t} + u\frac{\partial T}{\partial x} + v\frac{\partial T}{\partial y}\right) &= k\left(\frac{\partial^2 T}{\partial x^2} + \frac{\partial^2 T}{\partial y^2}\right) + \frac{\partial u}{\partial x}S_{xx} + \frac{\partial v}{\partial y}S_{yy} + \left(\frac{\partial u}{\partial y} + \frac{\partial v}{\partial x}\right)S_{xy} \\ &+ \rho_p c_p\left[\frac{D_T}{T_m}\left\{\left(\frac{\partial T}{\partial x}\right)^2 + \left(\frac{\partial T}{\partial y}\right)^2\right\} + D_B\left(\frac{\partial T}{\partial x}\frac{\partial C}{\partial x} + \frac{\partial C}{\partial y}\frac{\partial T}{\partial y}\right)\right] + \sigma B_o^2 u^2 - \frac{\partial q_r}{\partial y},\end{aligned} \tag{8}$$

$$\frac{\partial C}{\partial t} + u\frac{\partial C}{\partial x} + v\frac{\partial C}{\partial y} = D_B\left(\frac{\partial^2 C}{\partial x^2} + \frac{\partial^2 C}{\partial y^2}\right) + \frac{D_T}{T_m}\left(\frac{\partial^2 T}{\partial x^2} + \frac{\partial^2 T}{\partial y^2}\right) - k_1(C-C_0) \tag{9}$$

$$\frac{\partial F}{\partial t} + u\frac{\partial F}{\partial x} + v\frac{\partial F}{\partial y} = D_N\left(\frac{\partial^2 F}{\partial x^2} + \frac{\partial^2 F}{\partial y^2}\right) - \frac{b_1 W_c}{(C_1-C_0)}\left(\frac{\partial}{\partial x}\left(F\frac{\partial C}{\partial x}\right) + \frac{\partial}{\partial y}\left(F\frac{\partial C}{\partial y}\right)\right). \tag{10}$$

The boundary conditions are described below

$$u \pm \beta_1 S_{xy} = 0 \ \text{ at } y = \pm\eta, \tag{11}$$

$$\left[-\tau_1\frac{\partial^3}{\partial x^3}+m_1\frac{\partial^3}{\partial x\partial t^2}+d\frac{\partial^2}{\partial t\partial x}\right]\eta=\frac{\partial S_{xx}}{\partial x}+\frac{\partial S_{xy}}{\partial y}-\rho_f\left(\frac{\partial u}{\partial t}+u\frac{\partial u}{\partial x}+v\frac{\partial u}{\partial y}\right)-\sigma B_0^2u$$
$$+g(1-F_0)\rho_f\beta_T(T-T_0)-(\rho_p-\rho_f)g\beta_C(C-C_0)-(\rho_m-\rho_f)g\gamma(F-F_0)\text{ at } y=\pm\eta, \tag{12}$$

$$T\pm\beta_2\frac{\partial T}{\partial y}=\begin{Bmatrix}T_1\\T_0\end{Bmatrix},\ C\pm\beta_3\frac{\partial C}{\partial y}=\begin{Bmatrix}C_1\\C_0\end{Bmatrix},\ F=\begin{Bmatrix}F_1\\F_0\end{Bmatrix},\text{ at }\ y=\pm\eta, \tag{13}$$

where (u,v) are the components of the velocity in (x,y) directions, ν the kinematic viscosity, k the thermal conductivity, γ the average volume of microorganisms, p the pressure, ρ_f the density of the nanofluid, β_T is the thermal expansion coefficient, β_C is the mass expansion coefficient, D_T the thermophoretic coefficient of diffusion, W_c the maximum cell swimming speed, D_B the Brownian movement coefficient, d the coefficient of viscous damping, T_m the mean temperature, b_1 the chemotaxis constant,D_N the microorganisms diffusion coefficient, τ_1 the elastic tension, k_1 the rate of chemical reaction, $(\beta_1,\beta_2,\beta_3)$ the slip parameters, and m_1 the mass per unit area. T_1 and T_0 are the temperature at the upper and lower walls, respectively, and C_1 and C_0 are the concentration at upper and lower walls. (F_1,F_0) are the fraction's volume at the upper and lower walls. Further, the S_{xx}, S_{yy}, S_{yx}, S_{xy} extra stress tensor components are of Sutterby liquid.

The radiative heat flux q_r is depicted as

$$q_r=-\frac{4\bar{\sigma}}{3\bar{\kappa}}\frac{\partial T^4}{\partial y}, \tag{14}$$

where $\bar{\sigma}$ and $\bar{\kappa}$ represent the Stefan-Boltzmann absorption coefficients, where

$$T^4\cong 4T_0^3T-3T_0^4, \tag{15}$$

using (15) into (14), we get

$$q_r=-\frac{16\bar{\sigma}}{3\bar{k}}\frac{\partial T}{\partial y}. \tag{16}$$

The non-dimensional variables are the stream function ψ defined below [32]

$$\begin{aligned}&u=cu^*,\ v=cv^*,\ x=\lambda x^*,\ y=d_1y^*,\ ct=\lambda t^*,\ \eta=d_1\eta^*,\ u^*=\psi_y,v^*=-\delta\psi_x\\&d_1^2p=c\lambda\mu p^*,\ (T_1-T_0)\theta=T-T_0,\ (C_1-C_0)\phi=C-C_0,\ \beta_1^*d_1=\beta_1\mu,\\&d_1S_{ij}=\mu cS_{ij}^*,\beta_i^*d_1=\beta_i(i=2,3),(F_1-F_0)\chi=F-F_0,\ (F_1-F_0)\xi=F_0.\end{aligned} \tag{17}$$

The result we obtain after eliminating the asterisks and using the definitions above, along with an estimation of a long wavelength and small Reynolds number, is as follows:

$$\left[1-3B\left(\frac{\partial^2\psi}{\partial y^2}\right)^2\right]\frac{\partial^4\psi}{\partial y^4}-6B\left(\frac{\partial^3\psi}{\partial y^3}\right)^2\frac{\partial^2\psi}{\partial y^2}-M^2\frac{\partial^2\psi}{\partial y^2}+Gr\frac{\partial\theta}{\partial y}+Gc\frac{\partial\phi}{\partial y}+Gf\frac{\partial\chi}{\partial y}=0, \tag{18}$$

$$\left(\frac{1}{\Pr}+Rn\right)\frac{\partial^2\theta}{\partial y^2}+Nb\left(\frac{\partial\phi}{\partial y}\right)\left(\frac{\partial\theta}{\partial y}\right)+Nt\left(\frac{\partial\theta}{\partial y}\right)^2+Ec\left[\left(\frac{\partial^2\psi}{\partial y^2}\right)^2+M^2\left(\frac{\partial\psi}{\partial y}\right)^2-B\left(\frac{\partial^2\psi}{\partial y^2}\right)^4\right]=0, \quad (19)$$

$$\frac{\partial^2\phi}{\partial y^2}+\frac{Nt}{Nb}\left(\frac{\partial^2\theta}{\partial y^2}\right)-Sc\zeta\phi=0. \quad (20)$$

$$\frac{\partial^2\chi}{\partial y^2}-Pe\left(\chi\frac{\partial^2\phi}{\partial y^2}+\xi\frac{\partial^2\phi}{\partial y^2}+\frac{\partial\phi}{\partial y}\frac{\partial\chi}{\partial y}\right)=0. \quad (21)$$

The boundary conditions become

$$\frac{\partial\psi}{\partial y}\pm\beta_1\left[\frac{\partial^2\psi}{\partial y^2}-B\left(\frac{\partial^2\psi}{\partial y^2}\right)^3\right]=0 \text{ at } y=\pm\eta, \quad (22)$$

$$\left[E_1\frac{\partial^3}{\partial x^3}+E_2\frac{\partial^3}{\partial x\partial t^2}+E_3\frac{\partial^2}{\partial x\partial t}\right]\eta=\frac{\partial^3\psi}{\partial y^3}-3B\frac{\partial^3\psi}{\partial y}\left(\frac{\partial^2\psi}{\partial y^2}\right)^3-M^2\frac{\partial\psi}{\partial y}+Gr\theta+Gc\phi+Gf\chi \text{ at } y=\pm\eta, \quad (23)$$

$$\theta\pm\beta_2\frac{\partial\theta}{\partial y}=\begin{Bmatrix}1\\0\end{Bmatrix},\phi\pm\beta_3\frac{\partial\phi}{\partial y}=\begin{Bmatrix}1\\0\end{Bmatrix},\chi=\begin{Bmatrix}1\\0\end{Bmatrix} \text{ at } y=\pm\eta. \quad (24)$$

Note that (3) is satisfied automatically. Further, δ is the wave number, α the thermal diffusivity, Re the Reynolds number, ε the amplitude ratio, Pr the Prandtl number, Ec the Eckert parameter, ζ the chemical reaction variable, Rn the radiation parameter, Nt the thermophoresis parameter, B the Sutterby liquid variable, M the Hartman parameter, Nb the Brownian diffusion parameter, $(E_1\ E_2,\ E_3)$ the wall parameters, Pe the bioconvection Peclet number, Gf the bioconvection Rayleigh number, Gc the concentration Grashof number, Gr the thermal Grashof parameter, and Sc the Schmidt number, where

$$\begin{aligned}
&\delta=\frac{d_1}{\lambda},\ \alpha=\frac{k}{\rho_f c_f},\ \mathrm{Re}=\frac{\rho_f c d_1}{\mu},\ \varepsilon=\frac{a}{d_1},\ \Pr=\frac{\mu c_f}{k},\ Ec=\frac{c^2}{c_f\left(T_1-T_0\right)},\ \zeta=\frac{k_1 d_1^2}{\nu},\\
&Rn=\frac{16\bar{\sigma}T_0^3}{3\bar{\kappa}k},\ Nt=\frac{D_T\tau(T_1-T_0)}{T_m\nu},\ B=\frac{c^2m^*b^2}{6d_1^2},\ M=\sqrt{\frac{\sigma}{\mu}}B_0d_1,\ Nb=\frac{D_B\tau(C_1-C_0)}{\nu},\\
&E_2=\frac{cm_1d_1^3}{\lambda^3\mu},\ E_3=\frac{d_1^3d}{\lambda^2\mu},\ E_1=-\frac{d_1^3\tau}{\lambda^3\mu c},\ Pe=\frac{b_1W_c}{D_N},\ Gf=\frac{(\rho_m-\rho_f)g\gamma(F_1-F_0)d_1^2}{\mu c},\\
&Gc=\frac{g\beta_C(\rho_p-\rho_f)d_1^2(C-C_0)}{\mu_0 c},\ Gr=\frac{g\beta_T(1-F_0)\rho_f(T-T_0)d_1^2}{\mu c},\ Sc=\frac{\nu}{D_B}.
\end{aligned} \quad (25)$$

3. Numerical outcomes and discussion

The nonlinear equations (18)–(24) are tackled numerically by the NDsolve [9,20,32] technique in the software Mathematica. Here, we used a numerical technique because the exact solution of this system of equations is very much impossible. The numerical technique we employed here is built in the technique in Mathematica which offers a comprehensive toolset for symbolic and numerical computation, enabling users to solve complex mathematical problems accurately and efficiently.

3.1 Velocity

Figures 1–7 show the impacts of several parameters on the velocity profile. Figure 1 examines how the Sutterby fluid parameter B influences velocity. This indicates that a greater B increases the fluid's velocity. An increase in B lowers the fluid's resistance to flow due to its shear-thinning nature, which enhances the velocity. Figure 2 illustrates how the velocity slip variable β_1 affects velocity. The velocity of the material shows an enhancing behavior against the slip parameter β_1. This is due to boundaries offering less resistance to fluid motion. Effects of the thermal Grashof parameter Gr on the velocity profile are observed in Figure 3. The figure revealed that the velocity of the liquid is enhanced. The graphical representation of velocity against bioconvection Rayleigh number Gf is depicted in Figure 4. The velocity increases with increasing Gf. The velocity increases with the buoyancy ratio number Gc because stronger solutal buoyancy increases the overall force driving the flow, leading to a steeper velocity profile, as shown in Figure 5. The consequences of Hartman number M on velocity are demonstrated in Figure 6. A decreasing behavior is witnessed against M on velocity. The "Lorentz force" physically acts as a barrier within the flow field due to the magnetic field's presence. The impact of wall parameters E_1, E_2, and E_3 on the velocity profile is shown in Figure 7. It is found that the velocity of the material declines with an increase in E_1 and E_2 while it reduces for E_3.

3.2 Temperature

Figures 8–15 represent the temperature distribution graphs against several parameters. Figure 8 is designed to see the impacts of Grashof number Gr on the thermal field. It has been detected that the temperature of the liquid is enhanced because stronger buoyancy forces augment convection, leading to greater thermal energy distribution in the fluid. The dynamics of the bioconvection Rayleigh number Gf are outlined in Figure 9. An increasing trend is witnessed for larger values of bioconvection Rayleigh number Gf. As convection strengthens, more heat is retained and distributed within the fluid, causing an overall increase in the temperature profile. Effects of the Eckert parameter Ec are displayed in Figure 10. Temperature of the liquid increases with the increment of Eckert parameter Ec. In actuality, Ec is related to the rise in temperature caused by viscous dissipation effects. Figure 11 illustrates the aspects of the thermal slip parameter β_2 on thermal field. It has been noticed that temperature increases with an increase in the thermal slip parameter β_2. Dynamics of the Sutterby fluid parameter B are portrayed in Figure 12. Here, greater values of material parameter B lead to a decreasing thermal field behavior. Figure 13 exhibits the effects of Brownian motion Nb and thermophoresis Nt on the thermal field. Observations show that increasing the values of both parameters results in higher temperature. When these parameters have higher physical values, it leads to more random motion of nanoparticles from the wall into the liquid, which in turn causes a rise in temperature. Figure 13 illustrates how the radiation parameter Rn changes with temperature. It depicts those larger values of the radiation parameter reduce the temperature of the material. This happens as a result of the fluid's temperature being higher than that of the walls, which causes the temperature to drop as heat escapes. The effects of wall parameters E_1, E_2, and E_3 on temperature are shown in Figure 15. The thermal field of the liquid is enhanced by increasing the values of E_1 and E_2, while decreasing behavior is observed for E_3.

3.3 Concentration

Figures 16–20 show the nanoparticle concentration behavior against several parameters. Figure 16 points out the consequences of the buoyancy ratio variable Gc in Figure 16. The decline in behavior is observed in the concentration profile against the buoyancy ratio parameter Gc. This is due to stronger buoyancy due to concentration gradients that promotes more effective mixing and transport, thus lowering localized concentrations. Effects of thermophoresis Nt on the concentration profile are displayed in Figure 17. It is worth noting that as thermophoresis Nt increases the concentration of nanoparticles decreases. Physically, this occurs because thermophoresis causes particles to move away from hotter regions, potentially resulting in a decline in particle concentration. Figure 18 shows the consequences of the chemical reaction variable ζ on nanoparticle concentration, where a decreasing trend is witnessed against the chemical reaction parameter ζ. The impacts of mass slip parameter on nanoparticle concentration β_3 are pictured in Figure 19. From this graph, we can see that the concentration of the nanoparticles declines. The mass transfer rate between the bulk fluid and the boundary is impacted by the concentration drop brought on by the slip parameter. Figure 20 shows the importance of the complaint wall parameters E_{123} on concentration profile. Concentration improves for larger E_1 and E_2 , while showing a contrary trend for E_3.

3.4 Motile microorganism

Motile microorganism distribution against different pertinent parameters is displayed in Figures 21–24. Sutterby fluid parameter B features on the motile microorganism's density are illustrated in Figure 21. Here, we can see that the density of motile microorganisms is enhanced. It's due to the material properties of the fluid. The relationship between the density of motile microorganisms and the bioconvection constant ξ is seen in Figure 22. Larger values of bioconvection constant ξ clearly decrease the density of motile microorganisms. Bioconvective Rayleigh number Gf effects on the density of motile microorganisms are shown in Figure 23. Results reveal that the density of motile microorganisms declines. As Gf increases, the buoyant force due to microorganism density gradients intensifies, which enhances fluid motion. This stronger convective movement disperses the microorganisms more rapidly across the domain. Figure 24 portrays the features of bioconvection Peclet number Pe on motile microorganisms density. Clearly, the density of motile microorganisms weakens as the bioconvection Peclet variable Pe increases.

3.5 Rate of heat transfer

Table 1 shows the impacts of the thermal slip variable β_2, thermal Grashof number Gr, radiation parameter Rn, Sutterby fluid parameter B, Eckert parameter Ec, Brownian motion Nb, and bioconvective Rayleigh parameter Gf on heat transfer rate. It is noted that the rate of heat transfer increases with the increment of the thermal slip parameter β_2, thermal Grashof number Gr, and Eckert number Ec. It can also be detected that the heat transfer rate shows an opposite trend against the radiation parameter Rn and Brownian motion Nb. By increasing the values of the Sutterby fluid variable B, the rate of heat transfer improves. It's because of the liquid material properties. Further heat transfer rate shows a declining behavior against bioconvective Rayleigh number Gf.

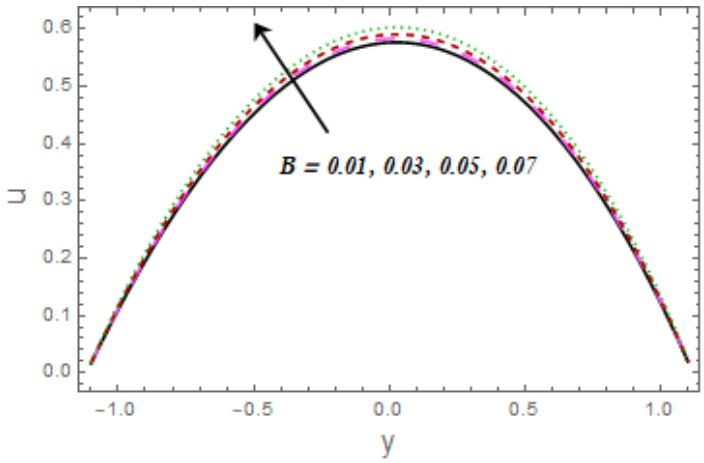

Figure 1. Variation of B on u.

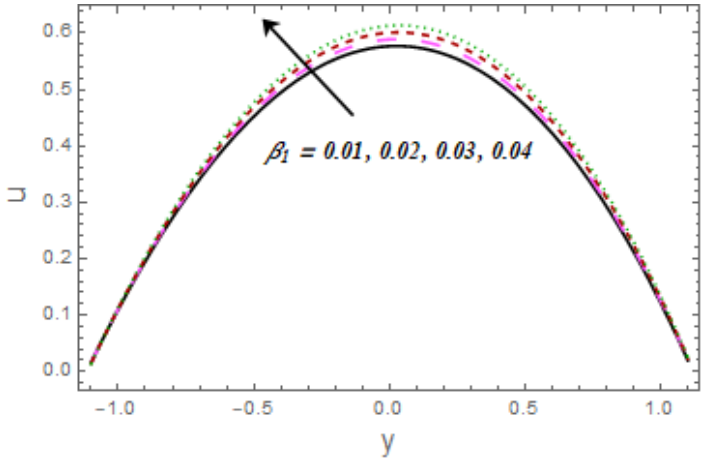

Figure 2. Variation of β_1 on u.

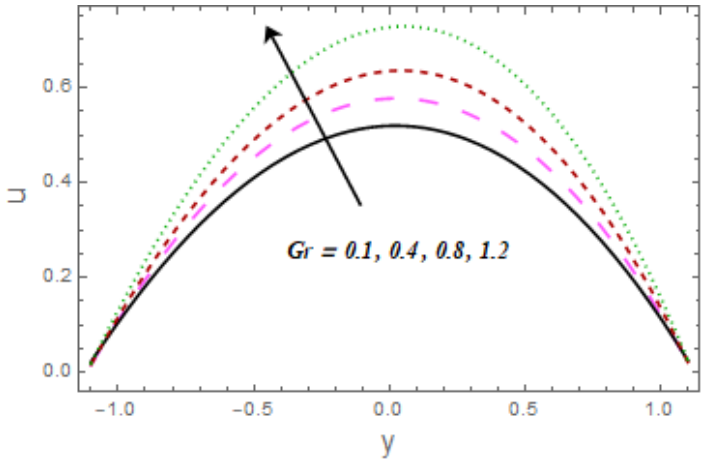

Figure 3. Variation of Gr on u.

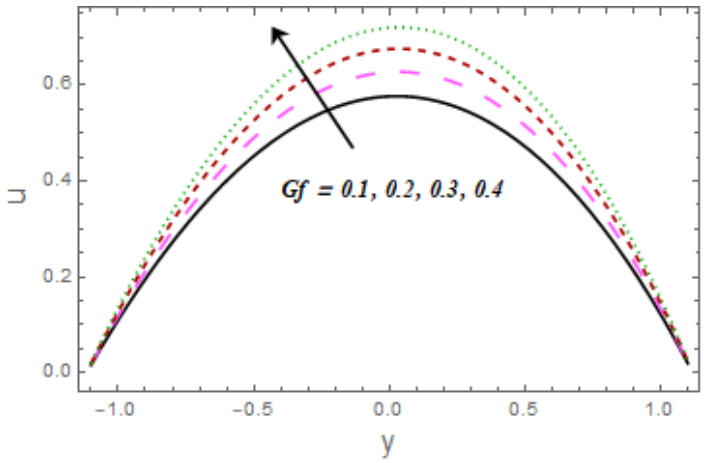

Figure 4. Variation of Gf on u.

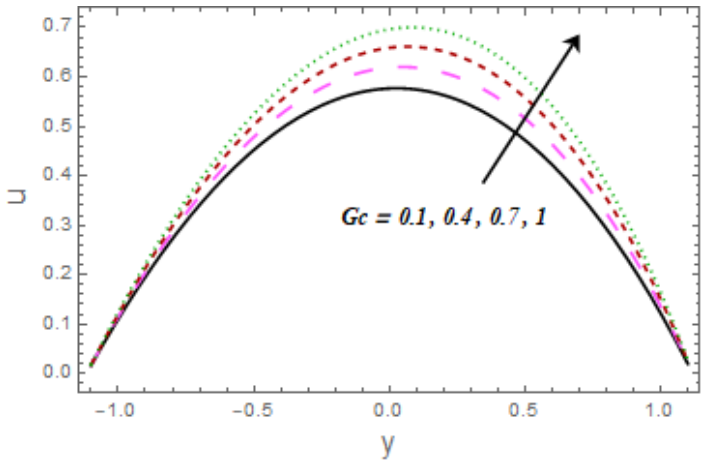

Figure 5. Variation of Gc on u.

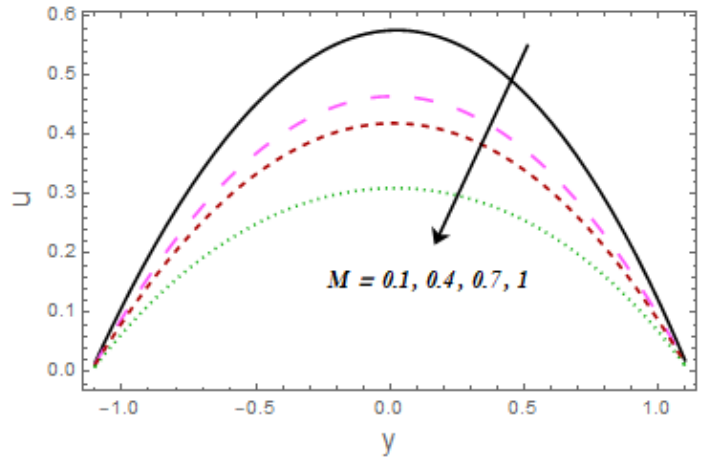

Figure 6. Variation of M on u.

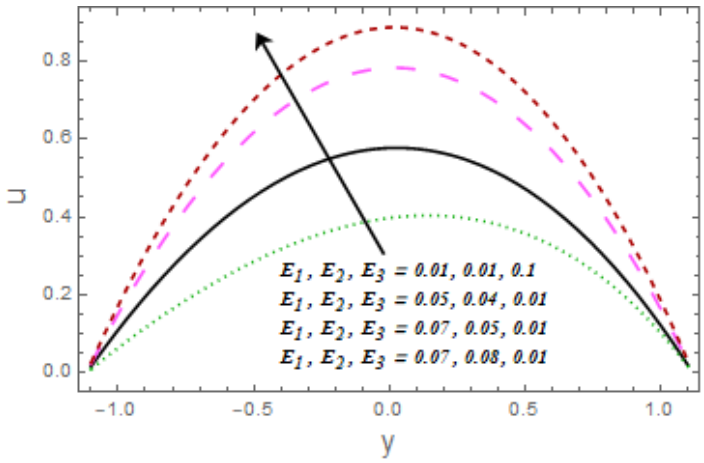

Figure 7. Variation of E_1, E_2, E_3 on u.

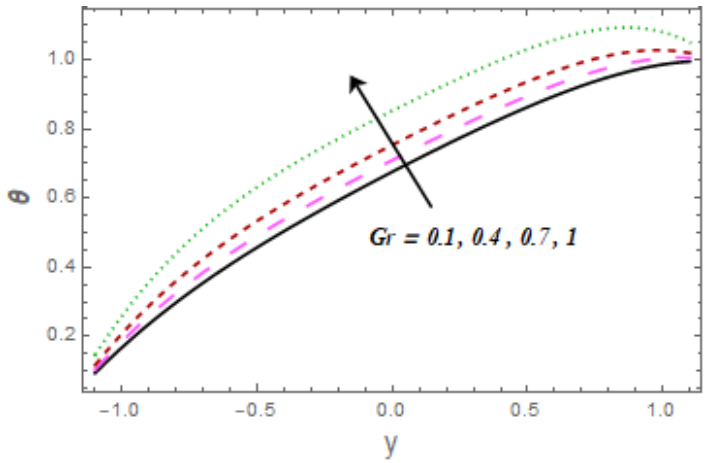

Figure 8. Variation of Gr on θ.

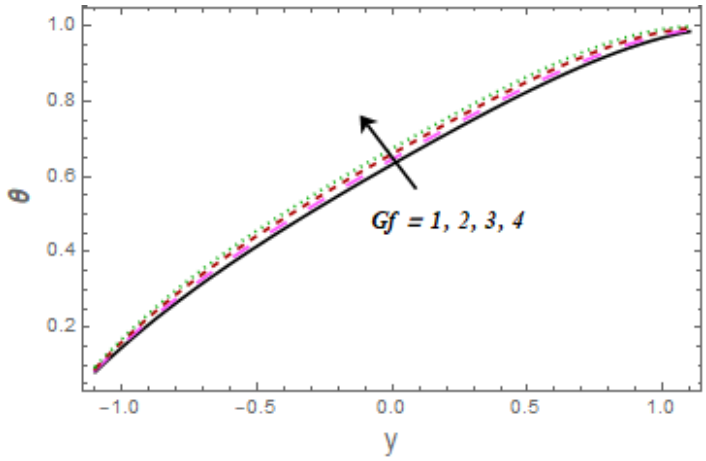

Figure 9. Variation of Gf on θ.

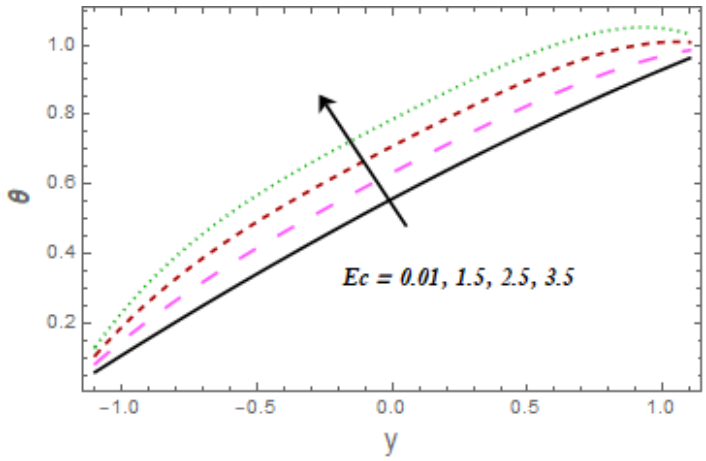

Figure 10. Variation of Ec on θ.

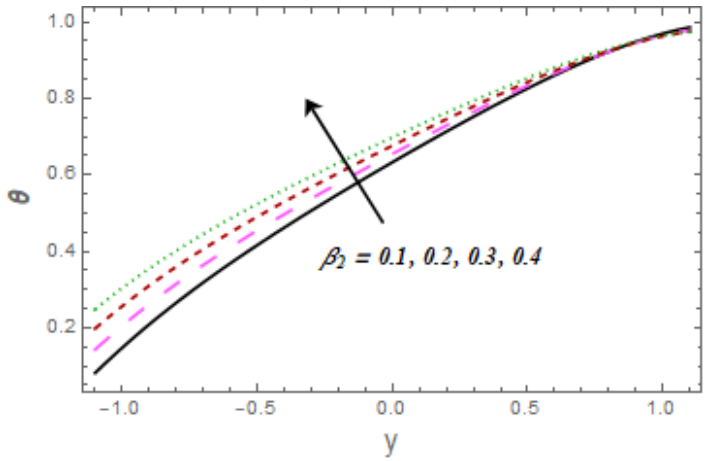

Figure 11. Variation of β_2 on θ.

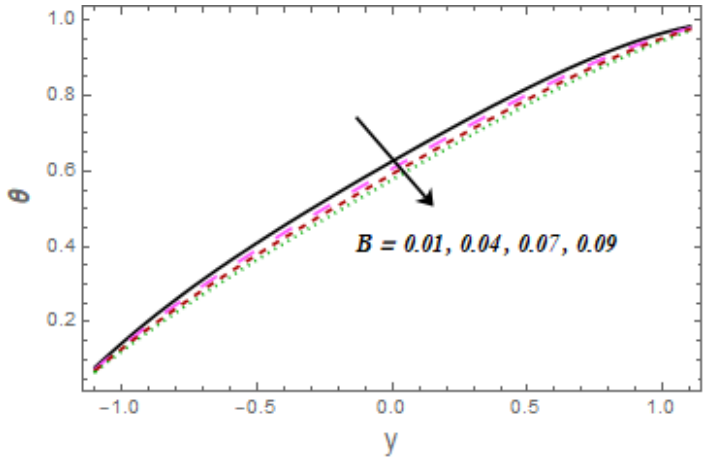

Figure 12. Variation of B on θ.

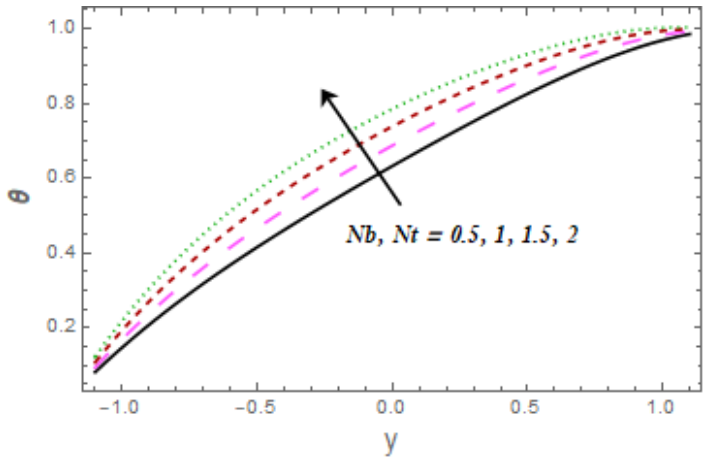

Figure 13. Variation of Nb, Nt on θ.

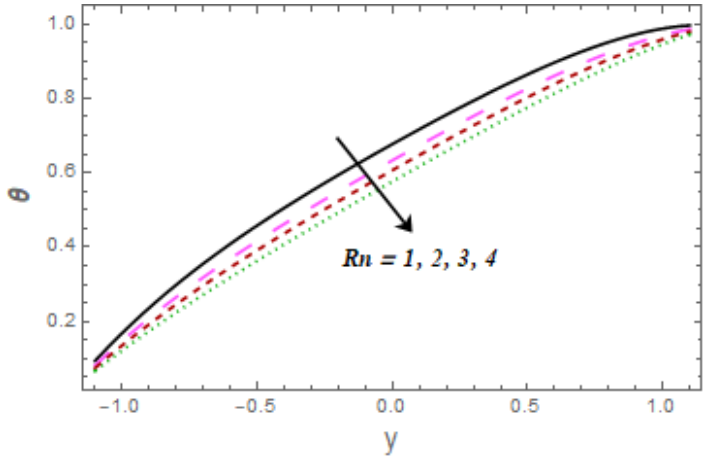

Figure 14. Variation of Rn on θ.

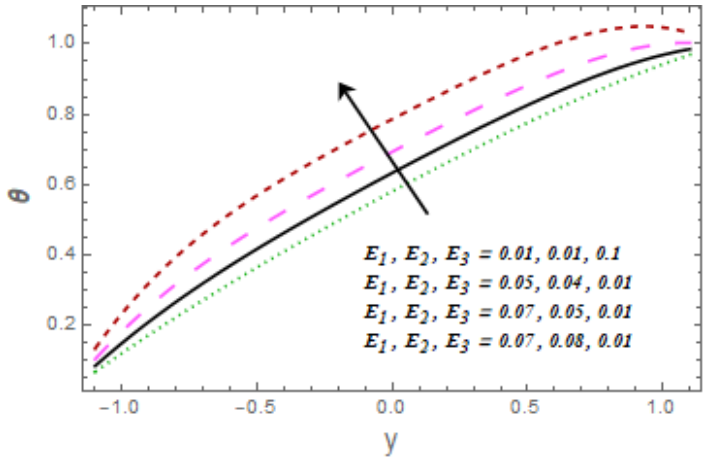

Figure 15. Variation of E_1, E_2, E_3 on θ.

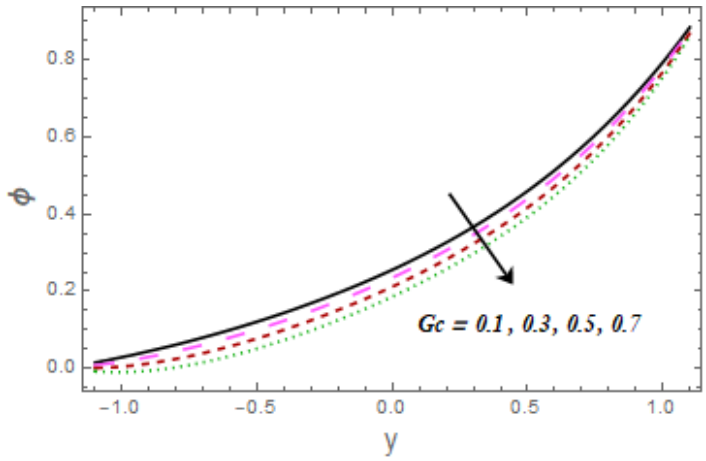

Figure 16. Variation of Gc on ϕ.

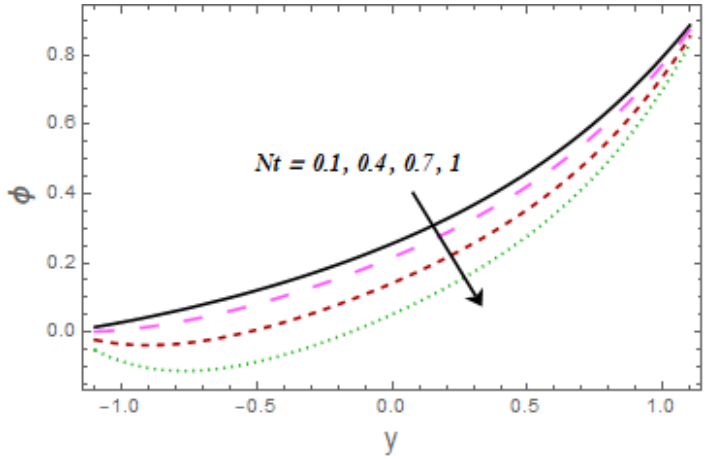

Figure 17. Variation of Nt on ϕ.

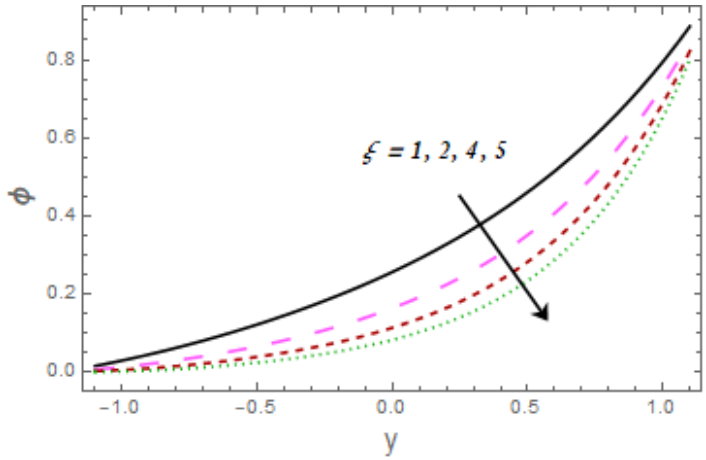

Figure 18. Variation of ξ on ϕ.

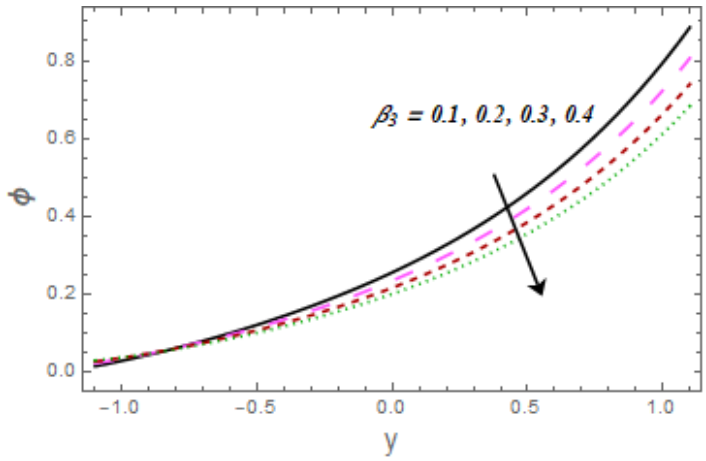

Figure 19. Variation of β_3 on ϕ.

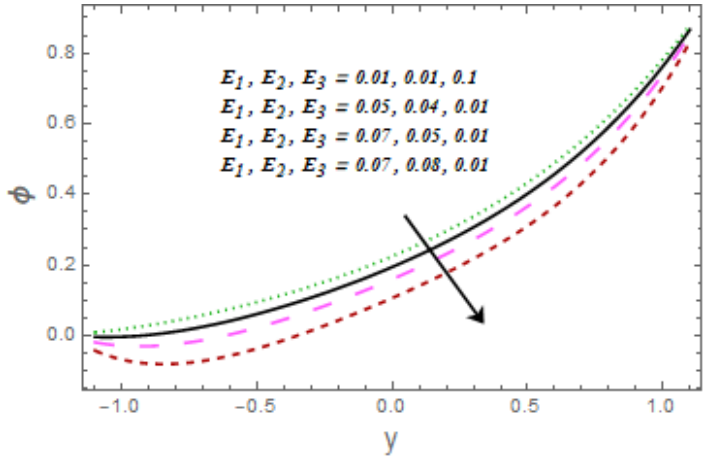

Figure 20. Variation of E_1, E_2, E_3 on ϕ.

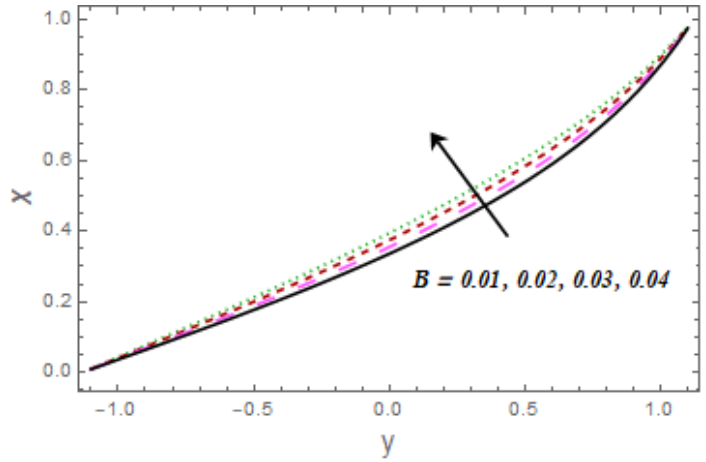

Figure 21. Variation of B on χ.

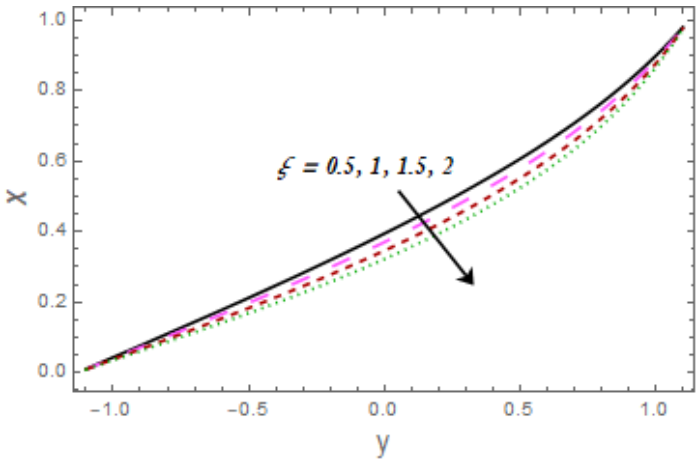

Figure 22. Variation of ξ on χ.

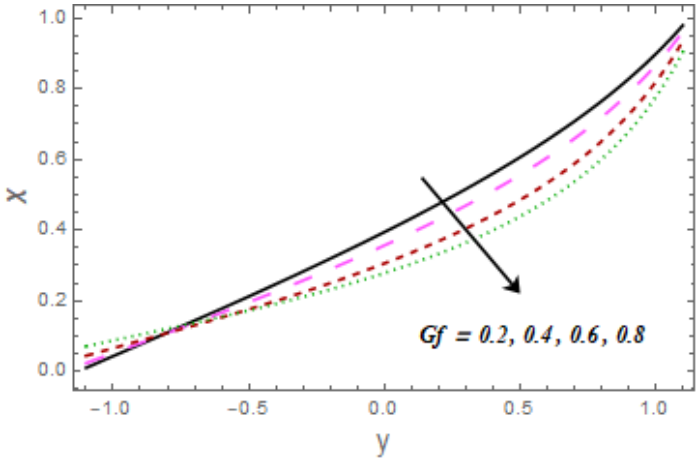

Figure 23. Variation of Gf on χ.

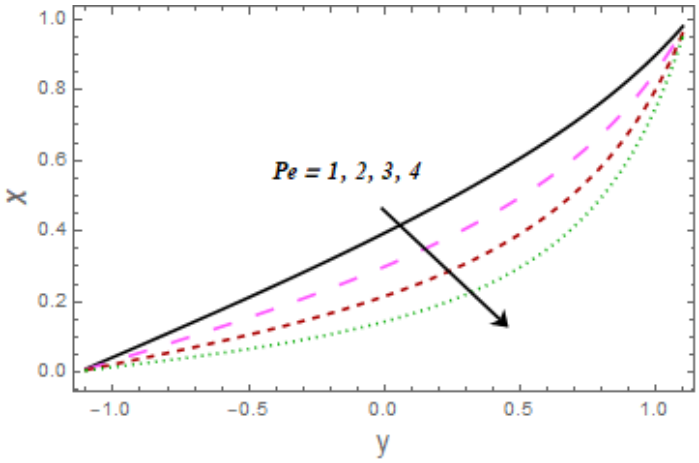

Figure 24. Variation of Pe on χ.

Table 1. Rate of heat transfer against different fixed values.

β_2	Gr	Rn	B	Nb	Ec	Gf	$-\theta'(\eta)$
0.1	0.5	1	0.02	0.5	1	0.1	0.08948
0.2							0.14220
0.1	**0.6**						0.18307
	0.8						0.22135
	0.5	**1.1**					0.06567
		1.3					0.02431
		1	**0.03**				0.00437
			0.04				0.00695
			0.01	**0.7**			0.11433
				1			0.13984
				0.5	**1.5**		0.32181
					2		0.57273
					1	**0.2**	0.10992
						0.4	0.06510

4. Validation

Table 2 shows the validation of the results when $Gc = Gf = Gr = M = Rn = B = \beta_1 = \beta_2 = \beta_3 = Sc = 0$. Results show good agreement with [34].

Table 2. Agreement of our numerical results with [34].

ε	η	Present study	Present study	Ref. [34]	Ref. [34]
		$\theta_y(\eta)$	$\phi_y(\eta)$	$\theta_y\ (\eta)$	$\phi_y\ (\eta)$
0.2	1.12	-0.211787	1.104644	-0.211789	1.104646
0.5	1.29	-5.523596	6.298790	-5.523598	6.298792

5. Conclusions

The current study investigates the bioconvection peristaltic flow of a Sutterby nanofluid. Thermal transport is influenced by the consequences of thermal radiation, Joule heating, and dissipation. Slip conditions are imposed on an elastic channel. The nonlinear system of equations is addressed using the numerical method. Here are the main findings of the study:

- Velocity is enhanced with an increase in velocity slip β_1 and thermal Grashof Gr parameters.
- The magnetic parameter Mleads to a resistance force causing the velocity to decrease.
- Velocity shows a similar trend against the Sutterby fluid parameter B and bioconvection Rayleigh number Gf.
- The temperature of the material shows an increasing behavior against the thermal Grashof parameter Gr and the Eckert number Ec.
- The thermal field shows an opposite trend against the radiation parameter Rn and the thermophoresis parameter Nb.

- Nanoparticle concentration decreases with the increment of the mass slip parameter β_3 and mass Grashof parameter Gr.
- First-order chemical reaction ζ shows a decreasing trend with concentration.
- The density of swimming microorganisms decreases the bioconvection Peclet number Pe.
- The rate of heat transfer boosts against Brownian motion Nb and Eckert parameters Ec.
- Future research could look at this endeavor in light of Cattaneo-Christov heat and mass fluxes, hybrid nanomaterials, and non-Newtonian model fluids.

Author contributions

Zahid Nisar: Writing−original draft, Methodology, Visualization, Software; Humaira Yasmin: Formal analysis, Writing–review & editing, Validation, Funding acquisition. All authors have read and approved the final version of the manuscript for publication.

Use of Generative-AI tools declaration

The authors declare they have not used Artificial Intelligence (AI) tools in the creation of this article.

Funding statement

This work was supported by the Deanship of Scientific Research, the Vice Presidency for Graduate Studies and Scientific Research, King Faisal University, Saudi Arabia (Grant No. KFU252458).

Conflict of interest

The authors declare no conflict of interest.

References

1. S. U. S. Choi, J. A. Eastman, Enhancing thermal conductivity of fluids with nanoparticles, In: *1995 International mechanical engineering congress and exhibition, San Francisco, CA (United States)*, 1995.
2. J. Buongiorno, Convective transport in nanofluids, *ASME J. Heat Transf.*, **128** (2006), 240–250. https://doi.org/10.1115/1.2150834
3. L. Godson, B. Raja, D. Mohan Lal, S. E. A. Wongwises, Enhancement of heat transfer using nanofluids-an overview, *Renew. Sustain. Energy Rev.*, **14** (2010), 629–641. https://doi.org/10.1016/j.rser.2009.10.004
4. A. M. Hussein, R. A. Bakar, K. Kadirgama, Study of forced convection nanofluid heat transfer in the automotive cooling system, *Case Stud. Therm. Eng.*, **2** (2014), 50–61. https://doi.org/10.1016/j.csite.2013.12.001
5. T. Hayat, S. Nadeem, Heat transfer enhancement with Ag-CuO/water hybrid nanofluid, *Results Phys.*, **7** (2017), 2317–2324. https://doi.org/10.1016/j.rinp.2017.06.034

6. M. A. Imran, A. Shaheen, E. M. Sherif, M. R.Gorji, A. H. Seikh, Analysis of peristaltic flow of Jeffrey six constant nano fluid in a vertical non-uniform tube, *Chin. J. Phys.*, **66** (2020), 60–73. https://doi.org/10.1016/j.cjph.2019.11.029
7. F. M. Abbasi, S. A. Shehzad, Magnetized peristaltic transportation of boron-nitride and ethylene-glycol nanofluid through a curved channel, *Chem. Phys. Lett.*, **803** (2022) 139860. https://doi.org/10.1016/j.cplett.2022.139860
8. M. Ajithkumar, P. Lakshminarayana, K. Vajravelu, Diffusion effects on mixed convective peristaltic flow of a bi-viscous Bingham nanofluid through a porous medium with convective boundary condition, *Phys. Fluids*, **35** (2023), 032008. https://doi.org/10.1063/5.0142003
9. Z. Nisar, T. Hayat, K. Muhammad, B. Ahmed, A. Aziz, Significance of Joule heating for radiative peristaltic flow of couple stress magnetic nanofluid, *J. Magn. Magn. Mater.*, **581** (2023), 170951. https://doi.org/10.1016/j.jmmm.2023.170951
10. M. Ajithkumar, R. Meenakumari, G. Sucharitha, M. V. Reddy, K. Javid, P. Lakshminarayana, Bioconvective peristaltic transport of hydromagnetic Sutterby nanofluid through a chemically activated porous channel with gyrotactic microorganisms, *J. Appl. Phys*., **135** (2024), 194701. https://doi.org/10.1063/5.0203027
11. Z. Nisar, B. Ahmed, M. E. Ghoneim, M. A. Elkotb, Thermal performance of mixed convective radiative peristaltic flow of Bingham nanofluid, *Sens. Actuators A: Phys.*, **373** (2024), 115399. https://doi.org/10.1016/j.sna.2024.115399
12. T. Hayat, S. Amjad, Z. Nisar, A. Alsaedi, Peristalsis of hybrid nanomaterial in convectively heated asymmetric configuration, *J. Therm. Anal. Calorim.*, **150** (2025), 175–185. https://doi.org/10.1007/s10973-024-13790-5
13. M. Sheikholeslami, N. Ataollahi, P. Scardi, M. A. Malagutti, Performance evaluation of a solar dish system with hybrid nanofluid cooling and sustainable thermoelectric power generation: Incorporating experimental property data, *Sol. Energy Mater.*, **285** (2025), 113508. https://doi.org/10.1016/j.solmat.2025.113508
14. T.W. Latham, Fluid motion in a peristaltic pump, *MS thesis, MIT Cambridge*, 1966.
15. A. H. Shapiro, M. Y. Jaffrin, S. L. Weinberg, Peristaltic pumping with long wavelength at low Reynolds number, *J. Fluid Mech.*, **37** (1969), 799–825. https://doi.org/10.1017/S0022112069000899
16. P. Trendelenburg, Physiological and pharmacological investigations of small intestinal peristalsis, *N-S Arch. Pharmacol.*, **373** (2006), 101–133. https://doi.org/10.1007/s00210-006-0052-7
17. A. Bandopadhyay, D. Tripathi, S. Chakraborty, Electroosmosis-modulated peristaltic transport in microfluidic channels, *Phys. Fluids*, **28** (2016), 052002. https://doi.org/10.1063/1.4947115
18. N. Imran, M. Javed, M. Sohail, P. Thounthong, Z. Abdelmalek, Theoretical exploration of thermal transportation with chemical reactions for sutterby fluid model obeying peristaltic mechanism, *J. Mater. Res. Technol.*, **9** (2020), 7449–7459. https://doi.org/10.1016/j.jmrt.2020.04.071
19. S. Akram, M. Athar, K. Saeed, A. Razia, Influence of an induced magnetic field on double diffusion convection for peristaltic flow of thermally radiative Prandtl nanofluid in non-uniform channel, *Tribol. Int.*, **187** (2023), 108719. https://doi.org/10.1016/j.triboint.2023.108719
20. Z. Nisar, T. Hayat, A. Alsaedi, S. Momani, Mathematical modelling for peristaltic flow of fourth-grade nanoliquid with entropy generation, *Z. Angew. Math. Mech.*, **104** (2024), e202300034. https://doi.org/10.1002/zamm.202300034
21. H. Alahmadi, J. Iqbal, F. M. Abbasi, Artificial neural network aided computing for two dimensional magnetohydrodynamic peristaltic movement of nanofluid with heat and mass transfer, *Eng. Appl. Artif. Intell.*, **154** (2025), 110990. https://doi.org/10.1016/j.engappai.2025.110990

22. S. Srinivas, J. B. Anasuya, V. Merugu, Interaction of pulsatile and peristaltic flow of a particle-fluid suspension with thermal effects, *Int. Commun. Heat Mass Transf.*, **163** (2025), 108728. https://doi.org/10.1016/j.icheatmasstransfer.2025.108728
23. M. Ishaq, M. B. Ashraf, M. U. Ashraf, S. Alshehery, A. A. Faqihi, H. M. Hadidi, Artificial neural network-based study of entropy optimization in Johnson-Segalman nanofluids through a peristaltic channel, *Phys. Fluids*, **37** (2025), 033103. https://doi.org/10.1063/5.0255518
24. J. L. Sutterby, Laminar converging flow of dilute polymer solutions in conical sections: Part I. Viscosity data, new viscosity model, tube flow solution, *AIChE J.*, **12** (1966), 63–68. https://doi.org/10.1002/aic.690120114
25. N. S. Akbar, S. Nadeem, Nano Sutterby fluid model for the peristaltic flow in small intestines, *J. Comput. Theor. Nanosci.*, **10** (2013), 2491–2499. https://doi.org/10.1166/jctn.2013.3238
26. S. I. Abdelsalam, A. Magesh, P. Tamizharasi, A. Z. Zaher, Versatile response of a Sutterby nanofluid under activation energy: hyperthermia therapy, *Int. J. Numer. Meth. Heat Fluid Flow.*, **34** (2024), 408–428. https://doi.org/10.1108/HFF-04-2023-0173
27. P. Chinnasamy, R. Sivajothi, S. Sathish, M. Abbas, V. Jeyakrishnan, R. Goel, et al., Peristaltic transport of Sutterby nanofluid flow in an inclined tapered channel with an artificial neural network model and biomedical engineering application, *Sci. Rep.*, **14** (2024), 555. https://doi.org/10.1038/s41598-023-49480-9
28. R. Revathi, T. Poornima, Dynamics of stagnant Sutterby fluid due to mixed convection with an emphasis on thermal analysis, *J. Therm. Anal. Calorim.*, **149** (2024), 7059–7069. https://doi.org/10.1007/s10973-024-12943-w
29. F. Ali, M. Kamal, M. Faizan, S. S. Zafar, Numerical treatment of the bio-convective Sutterby nanoliquid through a heat convective spinning disk, *Mod. Phys. Lett. B.*, **39** (2025), 2450471. https://doi.org/10.1142/S0217984924504712
30. J. R. Platt, "Bioconvection patterns" in cultures of free-swimming organisms, *Science*, **133** (1961), 1766–1767. https://doi.org/10.1126/science.133.3466.1766
31. C. S. K. Raju, S. M. Ibrahim, S. Anuradha, P. Priyadharshini, Bio-convection on the nonlinear radiative flow of a Carreau fluid over a moving wedge with suction or injection, *Eur. Phys. J. Plus*, **131** (2016), 409. https://doi.org/10.1140/epjp/i2016-16409-7
32. T. Hayat, Z. Nisar, A. Alsaedi, Bioconvection and Hall current analysis for peristalsis of nanofluid, *Int. Commun. Heat Mass Transf.*, **129** (2021), 105693. https://doi.org/10.1016/j.icheatmasstransfer.2021.105693
33. A. M. Aly, A. A. Hyder, Fractional-time derivative in ISPH method to simulate bioconvection flow of a rotated star in a hexagonal porous cavity, *AIMS Math.*, **8** (2023), 31050–31069. https://doi.org/10.3934/math.20231589
34. M. Mustafa, S. Hina, T. Hayat, A. Alsaedi, Influence of wall properties on the peristaltic flow of a nanofluid: analytic and numerical solutions, *Int. J. Heat Mass Transfer*, **55** (2012), 4871–4877. https://doi.org/10.1016/j.ijheatmasstransfer.2012.04.060